Bulletin of the JSME Vol.1, No.1, 2014
Mechanical Engineering Reviews

Phonon recycling

Seungha SHIN*, Corey MELNICK* and Massoud KAVIANY*
* Department of Mechanical Engineering, University of Michigan,
Ann Arbor, 48109 USA
E-mail: kaviany@umich.edu

Received 1 October 2013

Abstract
Following an introduction to the macro-level heat recirculation pioneered by Echigo, we introduce phonon recycling, especially in nonequilibrium conditions. We review the sources of nonequilibrium (i.e., hot) phonons and their assisted and unassisted absorptions leading to electronic excitations. We then review an example of phonon recycling in high-power current circuits using heterobarriers with potentials matching with the optical phonon energy. This integrated hot-phonon absorbing barrier (HPAB) can reduce the operating temperature, the net heat generation, and the power consumption of these devices.

Keywords : Phonon recycling, Waste heat recovery, Hot phonon, Electron-phonon interaction, Phonon energy conversion, Heterobarrier, Monte Carlo simulation, Entropy of electron-phonon energy conversion, Theoretical efficiency

1. Heat recirculation background

Heat recycling concepts have been used in many technologies, including combustion systems pioneered by Echigo (Hanamura et al., 1993) and broadly reviewed by Weinberg (1986). In the internal combustion engine, Hanamura and Nishio (2003) suggested a pistons design using a porous medium as the heat regenerator which causes the superadiabatic temperature, as shown in Figure 1(a). It is predicted that this heat recirculation significantly increases the engine efficiency. Figure 1(b) uses the same heat recirculating concept with a moving regenerator (SiC foam) (Park and Kaviany, 2002), and the trajectory of the regenerator and the piston top are shown. Figure 1(c) shows the extra work extracted due to the regeneration, in a turbocharged, diesel engine. In this example, the regenerator increases the predicted fuel efficiency from 43% to 53% (Park and Kaviany, 2002). Heat recirculation and local thermal nonequilibrium have also been used in the design of a superadiabatic radiant porous burner with distinct preheater and radiation corridors (Vandadi, et al., 2013).

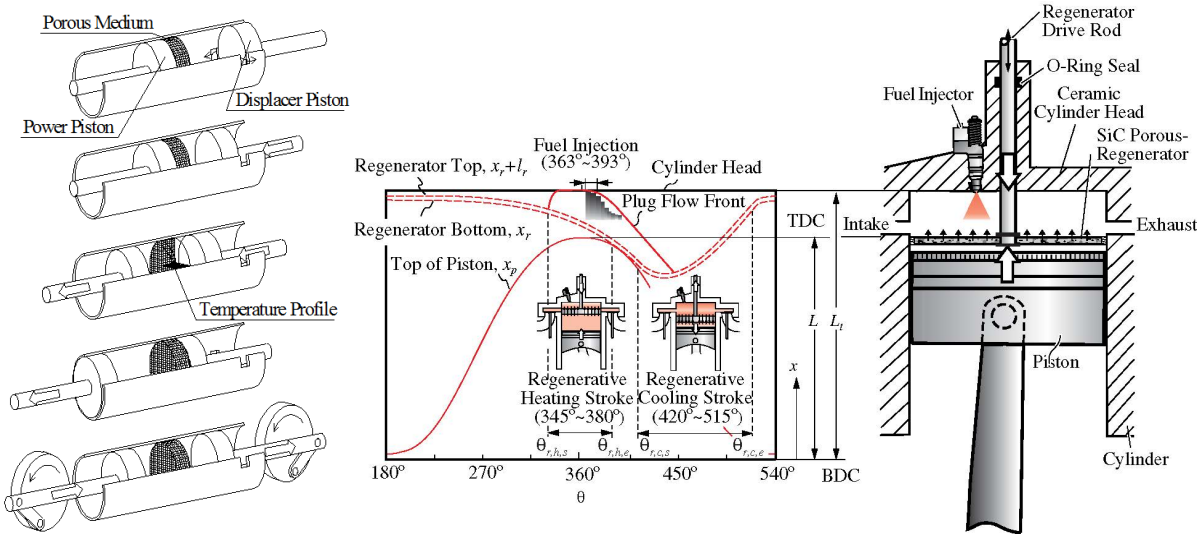

(a) (b)

Paper No.13-00246
[DOI: 10.1299/mer.2014tep0002]

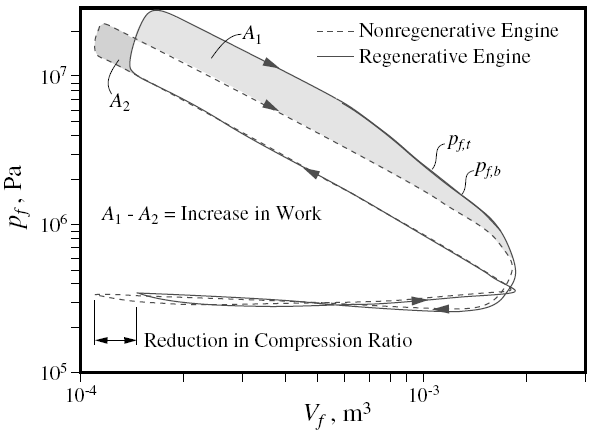

(c)

Fig. 1 (a) Schematic diagram of the superadiabatic combustion engine, showing the stationary regenerator and two pistons. From Hanamura and Nishio (Weinberg, 1986), reproduced by permission from *JSME*. (b) A movable, porous regenerator inside an internal combustion engine (Park and Kaviany, 2002), and (c) extra work extracted due to heat regeneration (Park and Kaviany, 2002), reproduced by permission from *ASME*.

2. Phonon recycling

While temperature expresses equilibrium atomic motion in fluid and solids, during energy conversion the populations (occupancies) of these kinetic energies are far from equilibrium. In solids with multiple atoms per primitive cell, the optical phonons which are the most energetic tend to be furthest from equilibrium population during the early periods of energy conversion (Kaviany, 2014) . The thermal nonequilibrium used in heat recirculation, has a counterpart at the atomic-level in phonon recycling (especially using nonequilibrium phonons). Although thermoelectric waste heat recovery research is rather established (Bell, 2008) and (Maldovan, 2013), the phonon recycling, which is based on the nonequilibrium carrier populations and pursues in-situ recovery processes (Kim and Kaviany, 2009), is new.

2.1 Source of Hot Phonons

Phonons are emitted by various decays, recombination and drags in energy conversions, and many resistive processes (e.g., in electronic circuits) (Fehr, et al., 2002), (Ridley, et al., 2004) and (Tsen, et al., 1996). Among the phonon modes, optical phonon emission is the dominant energy relaxation channel in semiconductors. The optical phonon emission rate can be larger than its decay rate, and the resulting optical mode overpopulation (over the equilibrium) is referred to as “hot phonons” (Kocevar, 1985). The sources of these hot optical phonon are presented in Fig. 2 and include the electric field induced acceleration of charges in high-power electronic devices (Matulionis, et al., 2004), nonradiative decay of hot electrons in optoelectric devices (Conibeer et al., 2010), lattice electron-stoppage of charged fission fragments (Goland and Paskin, 1964), frustrated-vibration relaxation of chemisorbed molecules (Sakong, et al., 2008), and magnetic field Landau splitting (Diaz-Pinto, et al., 2011). Some of these sources directly emit phonons, while others first excite an electric or magnetic entity which in turn decays, emitting phonons. These hot phonons are generally allowed to thermalize (reaching equilibrium occupancy), converting their energy to waste heat (equilibrium phonons) and generating entropy.

[DOI: 10.1299/mer.2014tep0002]

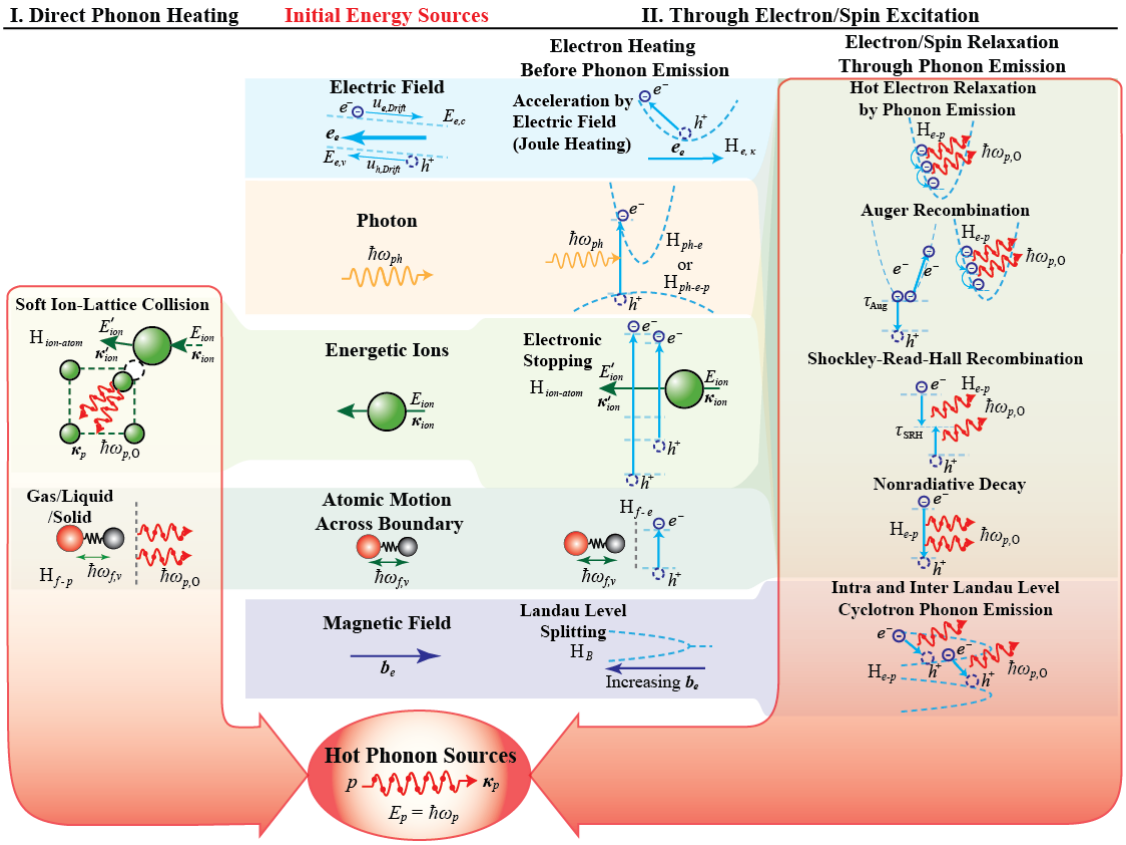

Fig. 2 Hot phonon emission from various sources. Optical phonons are emitted while electric potential, photon, energetic ion, molecular vibration, and magnetic energy are relaxed. With some sources phonons are directly emitted, and with others electron/spin system is first excited and then phonons are emitted during the electron/spin relaxation.

A large population of hot phonons leads to high temperatures, and also hinders the energy relaxation and transport, which are detrimental in most devices (Fehr, et al., 2002), (Ridley, et al., 2004). Therefore, device performance improves by proper consumption (assisted or unassisted absorption) of these hot phonons. Utilizing hot phonons before their thermalization is expected to be even more efficient, because of their lower entropy. However, due to small average speed of the optical phonons and the eminence of their downconversion to acoustic phonons, the hot phonons must be used quickly and close to their emission site.

2.2 Phonon recycling

Hot phonons can generate electronic potential after they interact with and are absorbed by electrons. This absorption can occur with or without assistance (i.e., mediation from a third energy carrier – usually photons). Figure 3 illustrates and classifies many of the important mechanisms. In the unassisted phonon absorptions, (1) - (3), a phonon collides with, is annihilated by, and transfers its energy to a charge carrier. In intraband transitions, the charge carrier gains kinetic and potential energy within its original band, while in the interband transitions it moves from one band to the other band. In particular, the interband transitions from the valence to the conduction band, a pair of electron-hole is created. In anti-stokes [phonon assisted cooling processes (4)-(6)], photon absorption requires the additional momentum and energy a phonon provides.

When design a system for phonon recycling or harvesting, we generally target one of these mechanisms. Each mechanism requires a distinct device design. For example, to generate electric potential through intravalley absorption (1), we use heterostructures (e.g., potential barriers) in a semiconductor to turn kinetic energy into potential energy. To recycle phonons generated in a laser, we choose ions with the precise electronic and vibrational properties and implant them around the lasing core (4). Finally, to generate charge pairs through unassisted phonon absorption (3), we must not only find or design materials with phonons more energetic than the electronic bandgap, but also create a device

[DOI: 10.1299/mer.2014tep0002]

which mimics that of a solar photovoltaic (SPV). We will briefly introduce such a device, the hot phonon voltaic (HPV), and demonstrate the need for in-depth and multi-scale.

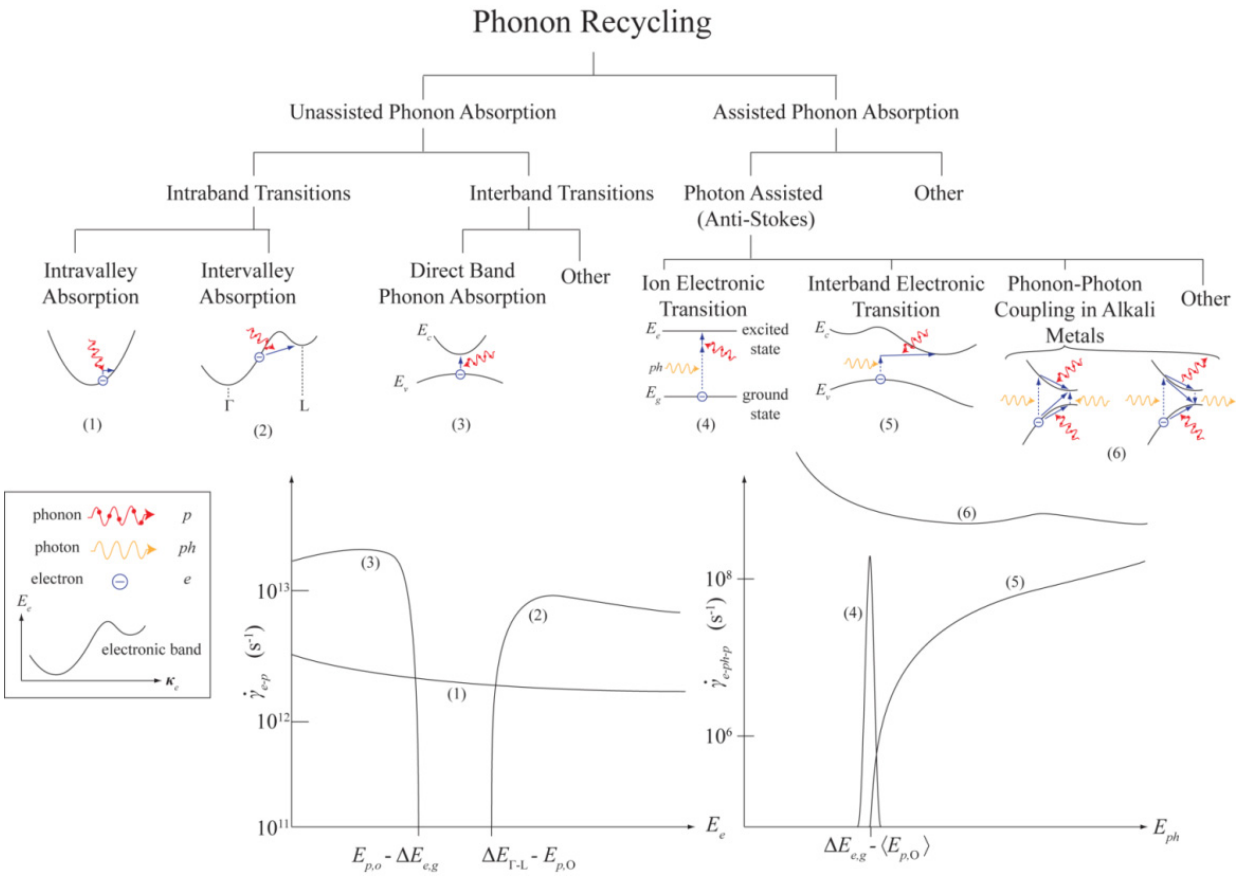

Fig. 3 Phonon recycling under unassisted and assisted absorptions. Each absorption is further classified by the electronic excitation it produces. These excitation are through the phonon-electron coupling. Typical rates for these transitions, indicating the strength of these couplings, are also shown. In phonon recycling the solid atomic and electronic structures are selected according to these functions.

In an SPV, photons generate charge pairs across a large bandgap (around 1 eV) which are then separated by, e.g., a *p-n* junction (Luque and Hegedus, 2011). A similar approach may be taken with the HPV. However, with a limited bandgap (phonon energies are typically limited to below 0.2 eV), it becomes exceedingly difficult to overcome the dark current and series resistances can often wash away potential gains. These problems are exacerbated as the temperature rises, and while in SPV these issues only have a moderate impact on efficiency, here they can destroy efficiency even at moderate temperatures. Moreover, while photon downconversion is negligible for visible and near-visible radiation, phonon downconversion is significant, especially as the temperatures rise. To minimize these issues, we require a material which both matches and maximizes phonon and electronic bandgap energy. Indeed, both atomic materials investigations and meso- or macroscale device simulation are required to design effective phonon recycling systems. Next, we detail exactly this process through the investigation of hot phonon absorption barriers, which utilize intraband phonon absorption processes, (1) and (2).

3. Hot-Phonon absorbing heterobarrier

3.1 Interaction kinetics of hot phonons

Phonons are scattered by boundaries, impurities and other energy carriers (i.e. phonon and electrons), and their energy can be exchanged with the electron system through the electron-phonon (*e-p*) interactions (Kaviany, 2014) . When targeting the hot phonons as the harvestable energy source, i.e., an electric potential, the *e-p* interaction which converts phonon to electron energy is emphasized.

[DOI: 10.1299/mer.2014tep0002]

The kinetics of hot phonon interactions can be calculated through quantum mechanical perturbation theory, i.e. the Fermi golden rule (FGR) (Kaviany, 2014) , (Lundstrom, 2000). For a single optical phonon interacting with an electron, we consider the perturbation by the atomic displacement, which is given as $d = [\hbar/(2m\omega_{p,\mathrm{O}})]^{1/2}(b^\dagger + b)$, where m is the reduced mass of oscillating atoms, $\omega_{p,\mathrm{O}}$ is the phonon frequency, and $b^\dagger$ (b) is the creation (annihilation) operator of phonon. Using the first order coupling $\varphi'_{e\text{-}p}$, the e-p interaction Hamiltonian $\mathrm{H}_{e\text{-}p} = \varphi'_{e\text{-}p}\,d$, and the interaction rate is expressed as

$$\dot{\gamma}_{e-p} = \frac{\pi}{m\omega_{p,\mathrm{O}}}\left|\left\langle \psi_{e,f} \mid \varphi'_{e-p} \mid \psi_{e,i} \right\rangle\right|^2 \left|\left\langle f_p \pm 1 \mid b^\dagger + b \mid f_p \right\rangle\right|^2 \delta_D(E_{e,f} - E_{e,i} \mp E_{p,\mathrm{O}}) \qquad (1)$$

where, ψ_e is the electron wave function, f_p is the phonon occupancy, δ_D is the Dirac delta function, E_e and E_p are the electron and phonon energy, and subscripts i and f represent the initial and final states. The matrix element $\left|\left\langle \psi_{e,f} \mid \varphi'_{e-p} \mid \psi_{e,i} \right\rangle\right|^2$ is estimated depending on the interaction type. For nonpolar optical phonon, it is $\phi'^2_{e-p}\delta_{\mathrm{D},\kappa}$, where ϕ'_{e-p} is the deformation potential and $\delta_{\mathrm{D},\kappa}$ is for the momentum conservation in e-p interaction. Since the lattice deformation perturbs the dipole moment between atoms in polar materials such as GaAs, polar nature should be considered in the interaction with longitudinal optical (LO) phonon, and thereby the matrix element becomes $(\rho e_c^2\omega_p^2/\kappa_p^2)(1/\varepsilon_{e,\infty} - 1/\varepsilon_{e,s})\delta_{\mathrm{D},\kappa}$, where $\varepsilon_{e,s}$ and $\varepsilon_{e,\infty}$ are the static and optical dielectric constants, e_c is the electron charge, κ_p is the phonon momentum, and ρ is the density[20]. Since $|\langle f_p \pm 1|b^\dagger + b|f_p\rangle|^2 = f_p + 0.5 \pm 0.5$, the phonon absorption and emission rates ($\dot{\gamma}_{p\to e}$ and $\dot{\gamma}_{e\to p}$) are proportional to f_p and $f_p + 1$, respectively.

Figure 4 shows the electron interaction rates in GaAs calculated by the FGR with experimental material properties, and it demonstrates that the polar optical (intravalley LO) phonon interaction is dominant for low-energy electrons in GaAs, which are heavily populated at room temperature. Also, phonon emission is possible only when the electron energy E_e is larger than phonon energy $E_{p,\mathrm{O}}$ (inset of Fig. 4), but the emission rate $\dot{\gamma}_{e\to p}$ increases with E_e faster than absorption $\dot{\gamma}_{p\to e}$. Thus, for a desirable condition for phonon absorption, we need to manipulate the electron population distribution to have large population of low-energy electrons (especially lower than $E_{p,\mathrm{O}}$).

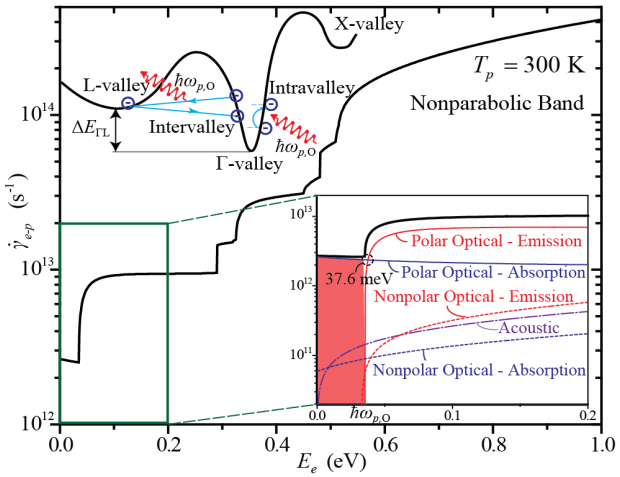

Fig 4. Variations of the electron interaction rates in the lowest conduction band, as a function of electron energy (E_e) for T_p = 300 K (Shin, et al., 2013). Insets show the band structure and various interaction mechanisms (left) and the interaction rates for low-E_e Γ-valley electrons (right). Polar optical phonon scattering is dominant at low E_e, and intervalley scattering rates increase with E_e. Reproduced by permission from *APS*.

3.2 Barrier composition

To create the electron distribution with large low-energy population favorable for phonon to electron energy conversion, a barrier structure was suggested (Shin, et al., 2013). Since only high-energy (or high-momentum) electrons can pass through the barriers, low-energy electrons are accumulated behind barrier creating the phonon-absorption favorable condition. The barrier structure can be formed by heterojunction composed of two different bandgap (E_g) materials, and GaAs/$\mathrm{Al}_x\mathrm{Ga}_{1-x}\mathrm{As}$ (x or x_{Al} is the Al content) structure is selected in Ref. 21. Due to the difference in bandgap between $\mathrm{Al}_x\mathrm{Ga}_{1-x}\mathrm{As}$ and GaAs ($E_{g,\mathrm{AlxGa1\text{-}x As}} > E_{g,\mathrm{GaAs}}$), a band-edge discontinuity in the

[DOI: 10.1299/mer.2014tep0002]

conduction and valence bands (ΔE_c and ΔE_v) appears at the interface, and it can be regarded as a potential barrier for charge carriers. As the discontinuity increases with x_{Al} ($\Delta E_c = 0.79x_{Al}$, $x_{Al} < 0.41$ and $\Delta E_v = -0.46x_{Al}$) (Ragay, et al., 1994) and (Zhu, et al., 1993), we control the barrier height φ_b by varying x_{Al}. Although a barrier stimulates phonon absorption, the potential change generates an adverse current. To compensate, a large, forward, and local electric field ($e_{e,HPAB}$) formed by x_{Al} grading follows the barrier to compensate this adverse effect (Shakouri and Bowers, 1997). The suggested hot-phonon absorbing barrier (HPAB) structure has a spatial distribution of x_{Al}, creating the electric field and potential distribution (barrier followed by large local field) as described in Fig. 5. Thereby, phonons are absorbed increasing electron kinetic energy, and this energy is, in turn, converted to potential through the barrier transition, while in thermionics (Kim, et al., 2010) and (Shakouri and Bowers, 1997), thermoelectrics (Shakouri, et al., 1998), and photovoltaics (Ragay, et al., 1994), the barrier structures have been considered for selective transmission (filtering) of the high-energy electrons (for thermoelectric performance enhancement) and heat absorption to restore the equilibrium electron distribution.

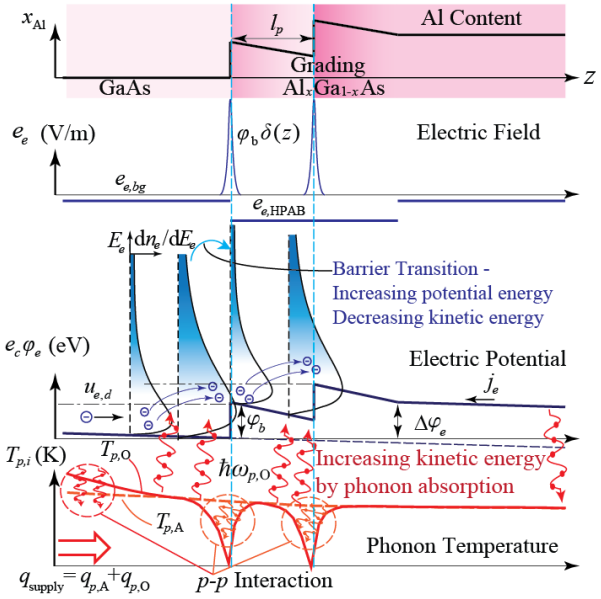

Fig. 5 Schematic of hot-phonon absorbing barriers (HPAB) and the spatial distributions of Al content, electric field and potential, and phonon temperatures (Shin, et al., 2013). x_{Al} abruptly increases, creating the potential barrier (with height φ_b) in the conduction band edge, while the grading maintains the current. Electrons with lower energy than the barrier height ($E_e > \varphi_b$) gain their kinetic energy through phonon absorption, and this energy is converted to electric potential. Reproduced by permission from *APS*.

3.3 Monte carlo simulations

The electric potential and power gain by the HPAB was tested by the self-consistent ensemble Monte Carlo (MC) method (Shin, et al., 2013). As the MC is generally employed to solve the Boltzmann transport equation (mesoscale) for energy carrier (Kaviany, 2014), the transport of sampled electrons (initially 200,000 electrons over 1 μm region) was simulated based on the electron interaction rates from first principles (Hess, 1991), (Jacoboni and Lugli, 1989), (Moglestue, 1993). The MC simulations demonstrated that the HPAB produces electric potential gain without current loss through a proper combination of $e_{e,HPAB}$, $f_{p,LO}$ (LO phonon population) and φ_b. The particle density and velocity distributions in the HPAB with a potential power gain prove the low-energy electron accumulation behind the barriers and the recovery of drift velocity by local field $e_{e,HPAB}$ as shown in Fig. 6(a).

The electric potential power gain (Δp_e) is the product of potential gain ($\Delta\varphi_e$) and the current density (j_e), and the absorbed phonon energy rate ($\dot{S}_{p\text{-}e}/A$) is given as

$$\frac{\dot{S}_{p-e}}{A} = \int_z \frac{\dot{S}_{p-e}}{V}\mathrm{d}z = \int_z \sum_j \int_{E_e} [\dot{\gamma}_{p\to e,j}(E_e) - \dot{\gamma}_{e\to p,j}(E_e)]E_{p,j}\frac{\mathrm{d}n_e(E_e)}{\mathrm{d}E_e}\mathrm{d}E_e\mathrm{d}z \qquad (2)$$

where j is an interaction mechanism and dn_e/dE_e (n_e: electron density) is the electron energy distribution. (Because of the large population at low E_e and no phonon emission with $E_e < E_{p,j}$, the large $\dot{S}_{p\text{-}e}/V$ is observed near the barrier.)

[DOI: 10.1299/mer.2014tep0002]

Then, the efficiency (of phonon energy conversion to electron) is defined as the ratio of the power gain and the absorbed phonon energy rate, $\eta_{p\to e} = \Delta p_e/(\dot{S}_{p\text{-}e}/A)$. The simulation results for various drift velocities $u_{e,d}$ and barrier heights φ_b (with the non-conserving lateral momentum (Kim et al., 2010) and (Vashaee and Shakouri, 2004)) show that $\eta_{p\to e,\max}$ is 18.8% when $u_{e,d} = 6.2\times10^4$ m/s and $\varphi_b = 30$ meV. For the continuous electric potential gain, the HPAB requires a sufficient phonon supply (otherwise phonon depletion reduces $T_{p,\mathrm{LO}}$ and the adverse current increases). The required phonon energy for various n_e and $\Delta\varphi_e$ is estimated from the simulations as in Fig. 6(b), and more $\dot{S}_{p\text{-}e}/A$ should be provided for the HPAB operation with larger n_e or $\Delta\varphi_e$,. The j_e with respect to n_e is also selected for high $\eta_{p\to e}$ (due to the dominant dependence of $\eta_{p\to e}$ on $u_{e,d}$). This demonstrates that large $\dot{S}_{p\text{-}e}/A$ (> 10^6 W/m^2) and j_e (10^6 to 10^{10} A/m^2) are necessary for high $\eta_{p\to e}$ with the conventional electron density ranges (10^{16} to 10^{18} cm^{-3}), and heat dissipation from some state-of-the-art integrated processors is in this range (F. J. Pollack, 1999).

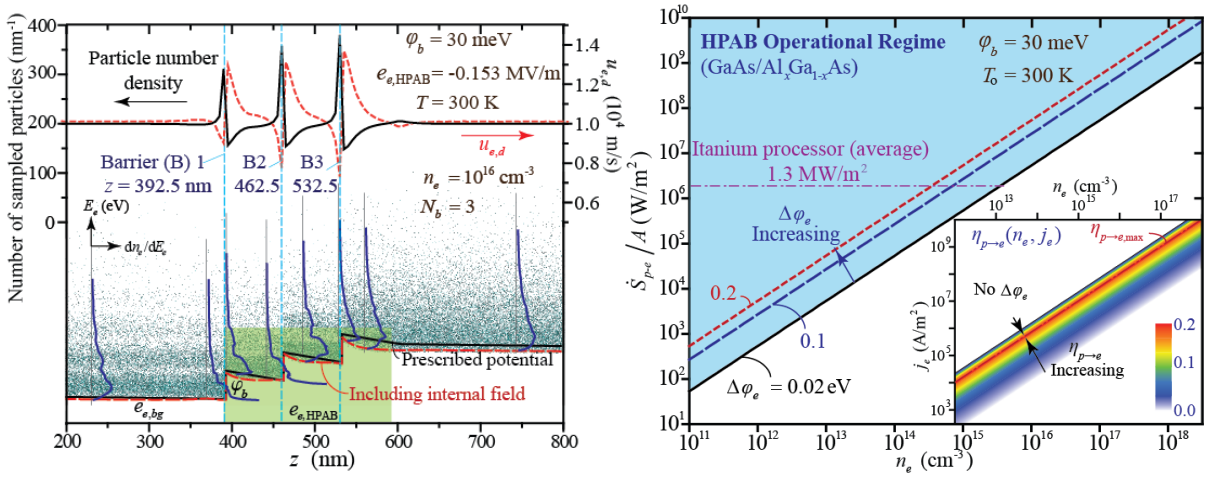

(a) (b)

Fig. 6 (a) Sampled particle number density, $u_{e,d}$, and particle-energy distribution over the simulation cell. Electrons are accumulated behind barriers and low-energy electrons are highly populated near barriers. (b) HPAB operational regime and variations of phonon energy absorption rate $\dot{S}_{p\text{-}e}/A$ with respect to n_e, for $\Delta\varphi_e = 0.02$, 0.1, and 0.2 eV, and $u_{e,d}$ $< 10^4$ m/s. Inset shows variations of $\eta_{p\to e}$ with respect to n_e and j_e. $\dot{S}_{p\text{-}e}/A$ (for a given $\Delta\varphi_e$ and j_e corresponding to $\eta_{p\to e,\max}$) increases with n_e. Reproduced by permission from *APS*.

3.4 Entropy analysis

The phonon energy conversion system using a heterobarrier (Shin, et al., 2013) was thermodynamically studied calculating the energy and entropy in electron and phonon subsystems (Shin and Kaviany, 2013). Since the energy distributions deviate from the equilibrium near the barriers, the nonequilibrium entropy should be addressed. Thus, we can use the statistical entropy of microstates rather than the one defined from temperature and heat flow in the classical thermodynamics. The statistical entropy (from the Boltzmann formulation (1964)) is $S = k_\mathrm{B}\ln W$, where k_B is the Boltzmann constant and W is the number of microstates for a given macrostate, and considering the properties of principal energy carriers, the phonon and electron entropies (S_p and S_e) are

$$S_p = \int_0^\infty k_\mathrm{B} D_p[(f_p+1)\ln(f_p+1) - f_p\ln f_p]\mathrm{d}E_p, \text{ and } S_e = -\int_{-\infty}^\infty k_\mathrm{B} D_e[(1-f_e)\ln(1-f_e) + f_e\ln f_e]\mathrm{d}E_e. \quad (3)$$

Here D_i is the density of states [per unit volume (or a primitive cell) and per unit energy range] and f_i is the occupancy function, and both D_i and f_i depend on carrier energy E_i ($i = e$ or p).

Using the statistical entropy and electron distribution, the particle number and energy conservation, the entropy production are examined for the 1D steady-state electron transport in HPAB. The control volume with a barrier at right boundary, as shown in Fig. 7(a), is analyzed. Under steady state, the electric current is consistent, so the electron number flux ($\boldsymbol{j}_{n,e}$, m^{-2}s^{-1}) at the left and right boundaries are the same, i.e.,

$$\Delta j_{n,e,z} = j_{n,e,R} - j_{n,e,L} = \int (u'_{e,d,R} D_e f_{e,R} - u'_{e,d,R} D_e f_{e,L})\mathrm{d}E_e = 0, \quad (4)$$

where $u'_{e,d}$ is the drift velocity at E_e and subscripts L and R represent the left and right boundaries. The change in the energy flux in the z direction is decomposed into phonon, electron potential, and electron thermal energy components

[DOI: 10.1299/mer.2014tep0002]

($\Delta q_{p,z}$, $\Delta p_{e,z}$ and $\Delta q_{e,z}$). The net phonon emission $\Delta q_{p,z}$ is $-\dot{S}_{p\text{-}e}/A$, the change in the electrochemical potential flux $\Delta p_{e,z}$ is $\Delta\varphi_e j_{n,e}$ ($\Delta\varphi_e = E_{F,R} - E_{F,L}$ and E_F is the Fermi level), and the electron heat flux change $\Delta q_{e,z}$ is $\int (q'_{e,R} - q'_{e,L})\mathrm{d}E_e$, where $q'_{e,R} = u'_{e,d,R(\mathrm{or}\,L)}[E_e - E_{F,R(\mathrm{or}\,L)}]D_{e,R(\mathrm{or}\,L)}f_{e,R(\mathrm{or}\,L)}$. Thus, with the energy conservation,

$$-\dot{S}_{p-e}/A + \int (q'_{e,R} - q'_{e,L})\mathrm{d}E_e + \Delta\varphi_e j_{n,e,z} = 0. \tag{5}$$

According to the second law of thermodynamics, the system entropy cannot decrease, i.e., $\Delta j_{S,e,z} + \Delta j_{S,p,z} \geq 0$, and it is also written as

$$\int (S'_{e,R}u'_{e,d,R} - S'_{e,L}u'_{e,d,L})\mathrm{d}E_e - \frac{\int (q'_{e,R} - q'_{e,L})\mathrm{d}E_e + \Delta\varphi_e j_{n,e,z}}{T_p} \geq 0. \tag{6}$$

Applying the left and right boundary electron energy distributions ($\mathrm{d}n_e/\mathrm{d}E_e$) to Eqs. (4), (5), and (6), the entropy production ($\Delta j_{S,z} = \Delta j_{S,e,z} + \Delta j_{S,p,z}$) can be calculated. $\mathrm{d}n_{e,L}/\mathrm{d}E_e$ is assumed in equilibrium, and $\mathrm{d}n_{e,R}/\mathrm{d}E_e$ is estimated using the barrier transition considering the energy and momentum conservation. As Fig. 7(b) shows, $\Delta j_{S,z}$ increases with $\Delta\varphi_e$ while $\eta_{p\to e}$ decreases. For the entropy production, the theoretical maximum efficiency ($\eta_{p\to e,\max}$) and potential gain ($\Delta\varphi_{e,\max}$) are found, when $\Delta j_{S,z} = 0$. When $T_p = T_e = 300$ K and $\varphi_b = 30$ meV, the predicted theoretical maximum efficiency is 41.6% with 16.0 meV as the maximum potential gain. With any carrier interactions, the entropy production should be larger than zero, therefore $\eta_{p\to e}$ in practical systems should be smaller than $\eta_{p\to e,\max}$. Thus, the non-ideal, irreversible MC simulation results for efficiency are also lower than this theoretical upper limit.

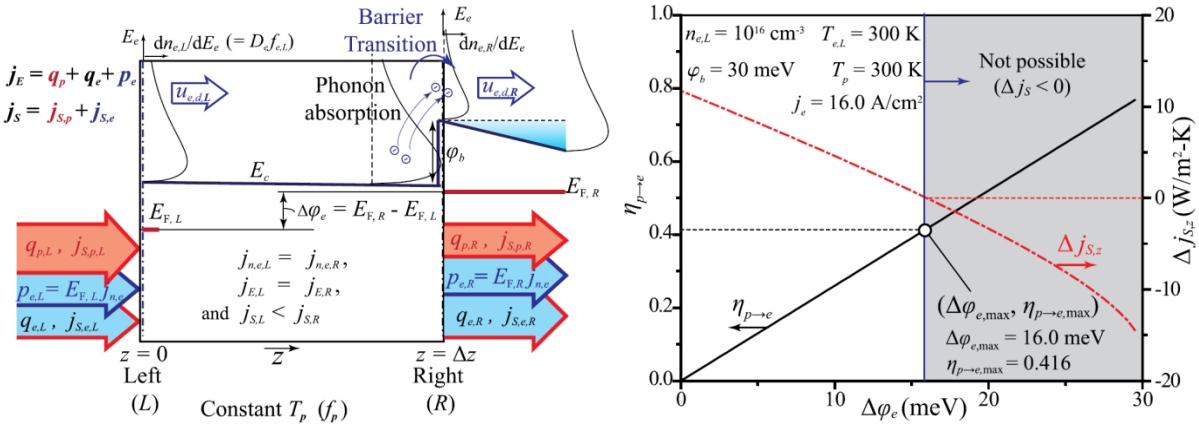

(a) (b)

Fig. 7 (a) The energy and entropy flux around the barrier structure with a 1D steady-state electrical current. The barrier is located just before the right boundary. Phonon temperature is prescribed as T_p, and the injected electron distribution ($\mathrm{d}n_{e,L}/\mathrm{d}E_e$) corresponds to equilibrium, while the exit distribution ($\mathrm{d}n_{e,R}/\mathrm{d}E_e$) is not. With electrochemical potential gain $\Delta\varphi_e$ ($= E_{F,R} - E_{F,L}$), entropy is produced in the system, conserving the electron number and energy. (b) Variations of energy conversion efficiency ($\eta_{p\to e}$) and the net entropy flux ($\Delta j_{S,z}$) with respect to the potential gain ($\Delta\varphi_e$). Here $\Delta j_{S,z}$ represents the entropy production rate per unit area in the 1-D transport system. The maximum efficiency ($\eta_{p\to e,\max}$) and potential gain ($\Delta\varphi_{e,\max}$) are found with $\Delta j_{S,z} = 0$. Reproduced by permission from *AIP*.

4. Conclusions

The suggested HPAB, which combines an abrupt barrier with a gradual potential decrease for favorable, unassisted phonon absorption, directly converts the phonon energy into harvestable electron potential, and it was studied by the numerical MC simulations and theoretical entropy analysis (Shin, et al., 2013), (Ragay, et al., 1994). This HPAB reverses the phonon role, which generally hinders electron transport, by harvesting hot phonons which would otherwise turn into waste heat. By integrating HPAB into electronic devices, reduced heat dissipation by the removal of excess phonons, as well as additional electric power generation (or recovery) will be achieved.

For the phonon recycling system design such as the HPAB and HPV, proper phonon energy and interaction kinetics, and compatible material pair for heterojunction should be selected. Figures 8(a) and (b) exemplify the optical

[DOI: 10.1299/mer.2014tep0002]

phonon energy spectrum in various materials, and the barrier height at the interface in GaX/AlGaX heterojunction structures for the HPAB (with respect to Al content). As for the hot phonon voltaic (HPV), the bandgap should be compatible to phonon energy for electron-hole pair creation, we can consider various energy conversion systems depending on the E_g as shown in Fig. 8(c).

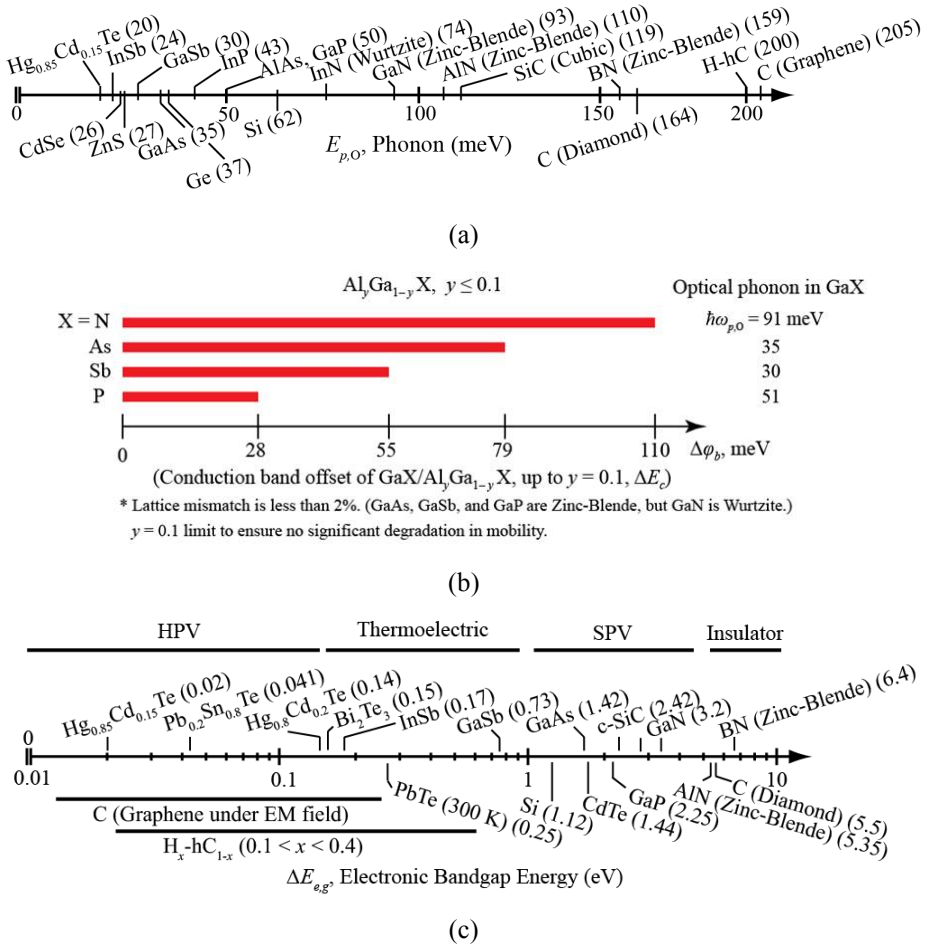

Fig. 8 (a) Optical phonon energy spectrum of some semiconductors. (b) Al-created heterobarrier with heights near the optical phonon energy, for four Ga compounds. (c) Bandgap energy of some semiconductors, and possible applications with respect to the bandgap.

Acknowledgments

The support by NSF Program on Thermal Transport and Processes, through Award CBET 1332807, and DOE, Office of Science, through Award DE-SC0000957 (CSTEC University of Michigan), are greatly appreciated.

References

Bell, L. E. , Cooling, heating, generating power, and recovering waste heat with thermoelectric systems, Science 321 (2008), 1457.

Boltzmann, L. , Lecture Notes on Gas Theory, Translated from the German Editions (Part 1; 1896, and Part 2; 1898) Dover, New York, (1964).

Conibeer, G. , Patterson, R. , Huang, L. , Guillemoles, J.-F., König, D. , Shrestha, S. and Green, M. , Modeling of hot carrier solar cell absorbers, Sol. Energ. Mat. Sol. Cells, 94 (2010), 1516.

Diaz-Pinto, C. , Lee, S., Hadjiev, V. G. and Peng, H. , Probing phonon emission via hot carrier transport in suspended graphitic multilayers, Solid State Communications 151 (2011), 1645–1649.

[DOI: 10.1299/mer.2014tep0002]

Fehr, J. N. , Dupertuis, M.-A. , Hessler T. P. , Kappei L. , Marti D., Salleras F. , Nomura M. S. , Deveaud B. , Emery J.-Y. and Dagens B., Hot phonons and Auger related carrier heating in semiconductor optical amplifiers, IEEE J. Quantum Elect. 38 (2002), 674.

Goland, A. N. and Paskin, A. , Model for fission fragment damage in thin polycrystalline metal films, J. Appl. Phys. 35 (1964), 2188.

Hanamura, K. , Echigo, R. , and Zhdanok, S.A. , Superadiabatic combustion in porous medium, Int. J. Heat Mass Transfer, 35 (1993), 3201.

Hanamura, K. and Nishio, S. , A feasibility study of reciprocating flow super-adiabatic combustion engine, JSME Series B, 46 (2003), 579 (2003).

Hess, K. , Monte Carlo Device Simulation: Full Band and Beyond, Kluwer Academic Publishers, Dordrecht, (1991).

Jacoboni, C. and Lugli, P. The Monte Carlo Method for Semiconductor Device Simulation, Springer-Verlag, Berlin, (1989).

Kaviany, M., Heat Transfer Physics, Second Edition, Cambridge University Press, New York, (2014).

Kim, J. and Kaviany, M. , Phonon recycling in ion-doped lasers, Appl. Phys. Lett. 95 (2009), 074103.

Kim, R. , Jeong, C. and Lundstrom, M. ,On momentum conservation and thermionic emission cooling, J. Appl. Phys. 107 (2010), 054502.

Kocevar, P. , Hot phonon dynamics, Physica B, 134 (1985), 155.

Lundstrom, M. , Fundamentals of Carrier Transport, Cambridge University Press, Cambridge, (2000).

Luque, A. and Hegedus s., Handbook of Photovoltaic Science and Engineering, Second Edition, Wiley, New York (2011).

Maldovan, M. , Sound and heat revolutions in phononics, Nature 503 (2013), 209.

Matulionis, A., Liberis, J., Matulionien, I., Cha, H. Y. , Eastman, L. F. and Spencer, M. G. , Hot-phonon temperature and lifetime in biased 4H-SiC, J. Appl. Phys., 96 (2004), 6439.

Moglestue, C. , Monte Carlo Simulation for Semiconductor Device, Chapman and Hall, London, (1993).

Park, C.-W. and Kaviany, M. , Evaporation-combustion affected by in-cylinder reciprocating porous regenerator, ASME J. Heat Transfer, 124 (2002), 184.

Pollack, F. J. , in MICRO'99: Proceedings of the 32nd Annual ACM/IEEE International Symposium on Microarchitecture (IEEE Computer Society, Washington, DC, USA, 1999), p. 2.

Ragay, F. , Ruigrok, E. and Wolter, J. , GaAs-AlGaAs Heterojunction Solar Cells with Increased Open-circuit Voltage, IEEE WCPEC. 2 (1994), 1934.

Ridley, B. K. , Schaff, W. J. and Eastman, L. F. , Hot-phonon-induced velocity saturation in GaN, J. Appl. Phys. 96 (2004), 1499.

Sakong, S. , Kratzer, P. , Han, X., Laß, K. , Weingart, O. and Hasselbrink, E. ,Density-functional theory study of vibrational relaxation of CO stretching excitation on Si(100), J. Chem. Phys. 129 (2008), 174702.

Shakouri, A. , Lee, E. , Smith, D. , Narayanamurti, V. and Bowers, J. , Thermoelectric effects in submicron heterostructure barriers, Microscale Thermophys. Eng. 2 (1998), 37.

Shakouri, A. and Bowers, J. , Heterostructure integrated thermionic coolers, Appl. Phys. Lett. 71 (1997), 1234.

Shin, S. , Melnick, C. and Kaviany, M. , Heterobarrier for converting hot-phonon energy to electric potential, Phys. Rev. B, 87 (2013), 075317.

Shin, S. and Kaviany, M. ,Entropy production in hot-phonon energy conversion to electric potential, J. Appl. Phys., 114 (2013), 083710.

Tsen, K. T. , Joshi R. P. , Ferry, D. K., A. Botchkarev, B. Sverdlov, A. Salvador, and H. Morkoç, Non-equilibrium electron distributions and phonon dynamics in wurtzite GaN, Appl. Phys. Lett. 68 (1996), 2990.

Vandadi, V. , Park, C. and Kaviany, M. Superadiabatic radiant porous burner with preheater and radiation corridors, Int. J. Heat and Mass Transfer, 64 (2013), 680.

Vashaee, D. and Shakouri, A. , Improved thermoelectric power factor in metal-based superlattices, Phys. Rev. Lett. 92 (2004), 106103.

Weinberg, F.A. , Editor, "Advanced combustion methods", Academic Press, London, (1986).

Zhu, Q. S. , Mou, S. M., Zhou, X. C. and Zhong, Z. T. , Determination of the conduction‐band offset of a single AlGaAs barrier layer using deep level transient spectroscopy, Appl. Phys. Lett. 62 (1993), 2813.

[DOI: 10.1299/mer.2014tep0002]